Geomechanics and Engineering, *Vol. 39, No. 3 (2024) 227-240*
https://doi.org/10.12989/gae.2024.39.3.227

Theoretical and numerical simulation analysis of the control effect of isolation piles on surface settlement induced by foundation pit excavation

Kunpeng Li[1a], Shihai Chen[*1], Peng Zhao[2b] and Rupeng Pei[2c]

[1]*College of Civil Engineering, Huaqiao University ,668 Jimei Avenue, Jimei District, Xiamen City, Fujian, China*
[2]*Xiamen Construction Engineering Co., Ltd. Of China Railway First Group., Xiamen, Fujian, China*

(*Received November 2, 2023, Revised August 23, 2024, Accepted October 10, 2024*)

Abstract. This study investigates the control effect of isolation piles on ground settlement resulting from foundation pit excavation. Based on the three-stage analysis method, first, the Kerr three-parameter foundation model is introduced, and the deflection differential equation is derived to solve the horizontal displacement of the diaphragm wall. Then, based on the horizontal displacement of the diaphragm wall, the boundary element method is used to calculate the additional stress at the boundary of the foundation pit, and the horizontal additional displacement and additional stress of the soil free field at the position of the isolation pile are obtained using the Mindlin solution. Subsequently, soil free field additional stress is applied to the pile foundation, and the shielding effect of group piles is also considered. Based on the Kerr three-parameter foundation model, the deflection differential equation of the pile foundation under the influence of horizontally oriented additional stress is established to solve the horizontal displacement of the isolated piles. Finally, the boundary element method is used again to invert the additional stress caused by the horizontal displacement of the isolation pile, and the surface settlement after the isolation pile is calculated in combination with the Mindlin vertical displacement solution. The spatial finite element model is established and compared with the theoretical calculation results to prove the rationality of the theory. The influence of basic construction parameters is analyzed theoretically, and it is found that the surface settlement is reduced by 30.9% compared with no isolation pile. Of the selected parameters in this paper, the effects of the isolation pile's controlled diameter, spacing, and elastic modulus, the thickness and elastic modulus of the diaphragm wall on the surface settlement are 4.9 mm, 3.1 mm, 3.3 mm, 3 mm, 1.7 mm, respectively, which are 45.4%, 28.7%, 30.6%, 27.8%, 15.7% of the standard working conditions, respectively. This shows that optimization of the isolation pile parameters has the best effect on surface settlement, optimization of the diaphragm wall parameters has the poor effect.

Keywords: boundary element method; foundation engineering; isolated piles; Kerr three-parameter foundation model; spatial finite element model; surface settlement control

1. Introduction

During the excavation of foundation pits, the enclosure structure often experience horizontal displacement and surrounding area often experience surface settlement. Managing these deformations, also known as deformation control, is a critical aspect of foundation pit engineering research. Isolation piles have emerged as a reliable and efficient protective measure for addressing this issue and are commonly employed in both foundation pit and tunnel engineering projects (Zheng *et al*. 2015). Despite the widespread use of isolation piles for deformation control in foundation pits, a comprehensive and systematic theoretical framework has yet to be developed. Therefore, there is a pressing need to establish a theoretical basis for the application of isolation piles in controlling surface settlement during foundation excavations.

Numerous studies have been conducted to investigate the functioning of isolation piles. The primary research methods employed include numerical simulation (Algin *et al.* 2022, Avci *et al.* 2023, Zheng *et al*. 2015, Rampello *et al*. 2019, Chen *et al*. 2016), laboratory experiments (Bilotta and Taylor 2005, Bilotta 2008, Chen *et al.* 2018), pile material improvement research (Stone *et al.* 2023, Visar Farhang *et al.* 2020), theoretical analyses (Gang *et al*. 2022, Cheng *et al.* 2019), and field measurements (Zheng *et al*. 2015, Chen *et al.* 2016). Bilotta (2008) utilized the centrifugal test method to examine the impact of diaphragm walls on the displacement field resulting from tunnel excavation. Stone *et al.* (2023) proposed a new composite foundation system, the caliche stiffened pile (CSP). Compared with a traditional deep foundation, it can improve the bearing capacity and settlement control ability of a pile foundation without changing the soil performance, optimizing the required pile length, and improving the economic benefits. Farhangi and Karakouzian (2020) used glass fiber-reinforced polymer (GFRP) filled with recycled and concrete material to replace traditional steel reinforced piles in bridge foundations and analyzed their structural responses. Avci and Ekmen (2023) used numerous

∗Corresponding author, Professor
E-mail: cshblast@163.com
[a]Ph.D.
[b]Ph.D. Student
[c]Senior Engineer
[d]Senior Engineer .

ISSN: 2005-307X (Print), 2092-6219 (Online)

parametric three-dimensional finite element analyses to optimize the parameters of the rammed aggregate pier-supported raft foundation, combined with the artificial intelligence-supported novel Goal Attainment Method and the Response Surface Method, the optimal design of the general raft foundation-rammed bone pier group system was finally realized. Rampello *et al.* (2019) conducted a study in which diaphragm walls and isolation piles were used to isolate the soil behind the piles individually. Finite element models were established to assess isolation pile effectiveness in both cases. Bilotta and Russo (2011) conducted a numerical simulation study to examine the protective effect of isolation piles on surrounding buildings during tunnel excavation.

Researchers have made significant progress in studying the theory of settlement control using isolation piles. Ledesma and Alonso (2017) utilized an analytical approach to address the vertical deformation of soil, considering the influence of isolation piles. Cao *et al.* (2022, 2023) introduced a simplified calculation method for determining the vertical displacement of surroundings induced by isolation piles during tunnel excavation. This method considers both the relative sliding of the pile–soil interface and the pile–soil interaction. Huang *et al.* (2022) developed an analytical solution for the surface settlement resulting from adjacent seismic isolation piles. Their solution was derived by incorporating Melan's solution and Loganathan's formula into their analysis. Nevertheless, the theories proposed in previous studies (Cao *et al*. 2022, 2023, Huang *et al.* 2022) primarily focus on the frictional effects around the pile foundation, disregarding the isolation effect exerted by the isolation pile itself. It should be noted that the isolation effect plays a crucial role in soil settlement control and can have a substantial impact on surface settlement following pile installation. Furthermore, these theories do not account for the deformation of the isolation pile itself. Cheng *et al.* (2019) examined the isolation effect of isolation piles on soil displacement induced by pit excavation. Zhang *et al.* (2019) introduced a two-stage time domain method to predict the viscoelastic interaction between a deep foundation pit and an adjacent pile foundation. Li *et al.* (2023a, b) employed a combination of local plastic deformation theory and the Mindlin solution to estimate the additional stress experienced by passive piles during the process of excavation. However, their analysis primarily focused on the impact of isolation piles on horizontal soil displacement and did not thoroughly investigate post-pile settlement.

In summary, isolation piles serve as an important means of controlling surface settlement around foundation pits, although there has been some theoretical research in recent years, the theoretical framework remains incomplete. First, the partitioning effect of isolation piles, the most important factor in controlling surface settlement, has not yet been reflected in the theoretical framework. Second, isolation piles are typically composed of a group of piles. Existing theories regarding the control of surface settlement by isolation piles do not take into account the shielding effect of the pile group. Finally, to accurately reflect the control effect of isolation piles on surface settlement caused by foundation pit excavation, the precision of additional stress calculations near the isolation piles is crucial. Existing studies calculate the additional stress based on the unloading due to foundation pit excavation, neglecting the impact of the diaphragm wall structure, which clearly leads to significant errors.

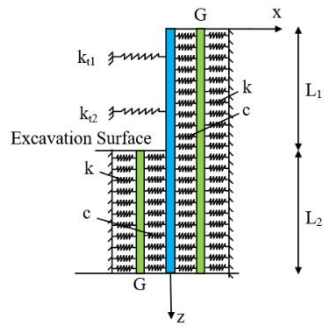

Fig. 1 Kerr three-parameter foundation model

Considering the problems in the existing theories, this paper proposes a new theory for calculating settlement control by isolation piles, fully considering the isolation role of isolation piles and the shielding effect of group piles, and solving the insufficiency of existing isolation pile theories. The boundary element method and Mindlin solution are introduced when calculating the additional stress caused by pit excavation to establish the relationship between the horizontal displacement of the diaphragm wall and the additional stress of the soil body, to improve the accuracy of the calculation of the additional stress, and to provide the basis for the theory accuracy. By analyzing the influence of each parameter on surface settlement, this theory provides guidance for selecting the parameters of isolation piles.

2. Calculation of additional soil stress around an isolation pile under the influence of foundation pit excavation

2.1 Calculation of horizontal displacement of the diaphragm wall

Various methods have been proposed for calculating the horizontal displacement of the diaphragm wall. These include the Winkler elastic foundation beam method (Xu *et al.* 2011), the Pasternak two-parameter foundation model method (Pasternak 1954, Zhu *et al.* 2022), and the Kerr three-parameter foundation model method (Kerr 1985). Among these methods, the Kerr three-parameter foundation model offers the advantage of comprehensively considering the shear characteristics of the soil, leading to higher calculation accuracy.

By considering the continuity of stress and deformation between the diaphragm wall and the soil, a comprehensive analysis model is established for the support structure of the inner support diaphragm wall, as illustrated in Fig. 1. In the diagram, k_t represents the stiffness coefficient of the elastic fulcrum of the inner support, L_1 denotes the length of the wall

above the excavation surface, and L_2 represents the length of the wall below the excavation surface.

In the analysis model, the soil adjacent to the diaphragm wall is modeled as an equivalent soil spring. To capture the shear force generated by the soil, a shear layer is introduced. The compression force exerted by the soil is accounted for using soil springs k and c. Additionally, the supporting force is considered by incorporating k_t into the analysis model.

In this calculation model, determination of the earth pressure is based on the static earth pressure theory. According to this theory, positive horizontal displacement (w) of the diaphragm wall corresponds to active deformation of the soil, while negative horizontal displacement corresponds to passive deformation of the soil. When active deformation of the soil occurs, the soil pressure increment is negative, whereas the internal support pressure increment is positive. Conversely, when the soil experiences passive deformation, the earth pressure increment is positive, and the internal support pressure increment is negative.

In the Kerr three-parameter foundation model, the variations in soil pressure and internal support pressure are taken into account and incorporated into the model. By treating the excavation face as the interface, separate deflection differential equations are established for the shear layer in the load-bearing section above the excavation face and the embedded section below the excavation face. The deflection differential equation of the loaded section is expressed as Eq. (1)

$$\begin{aligned} &-\frac{EIG_i}{c_i}\frac{d^6w_2}{dz^6}+\frac{EI\left(c_i+k_i\right)}{c_i}\frac{d^4w_2}{dz^4}-G_id\frac{d^2w_2}{dz^2}\\ &-\left(P_i-k_iw_2\right)d+k_{t_i}w_2+\frac{k_{ti}\left(c_i+k_i\right)}{c_i}w_2=0 \end{aligned} \tag{1}$$

The bending differential equation of the embedded section is expressed as Eq. (2)

$$\begin{aligned} &-\frac{EIG_i}{c_i}\frac{d^6w_2}{dz^6}+\frac{EI\left(c_i+k_i\right)}{c_i}\frac{d^4w_2}{dz^4}-\\ &2G_id\frac{d^2w_2}{dz^2}+2k_iw_2d-\Delta P_id=0 \end{aligned} \tag{2}$$

where P_i is the static soil pressure behind the wall above the excavation surface (kN/m), k_{ti} is the coefficient of the modulus of elasticity of the internal support, and ΔP_i is the difference in static soil pressure on both sides of the embedded section of the diaphragm wall (kN/m).

In the calculation parameters of the Kerr three-parameter foundation model, the stiffness coefficient of the elastic fulcrum of the inner support is selected according to Ma and Liang (2018). For the shear modulus G, the empirical formula proposed by Tanahashi (2004) is used for the calculation. The thickness of the shear layer can be selected according to Yao and Yin (2010). The foundation reaction force k is calculated using the foundation reaction modulus formula proposed by Vesic (1961). By utilizing the finite difference method and incorporating the boundary conditions at the top and bottom of the wall as well as the continuity conditions at the excavation surface.

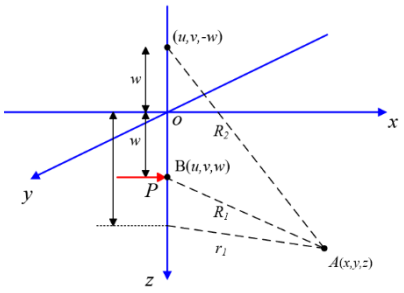

Fig. 2 Calculation model of soil displacement

2.2 Calculation of the horizontal additional stress on the foundation pit boundary

In the analysis of the horizontal displacement of the soil free field induced by excavation of the foundation pit, the boundary element method is employed. Based on this method's fundamental principles, the virtual force imposed on the boundary of the foundation pit leads to the generation of virtual stress and displacement fields in the surrounding soil. When the boundary conditions within the virtual displacement field align with the actual boundary conditions of the displacement in the foundation pit, it can be considered that the virtual displacement and stress fields reflect the boundary effect resulting from the excavation. Mindlin (1936) provided a displacement solution at any position when a horizontal concentrated load is applied in an elastic semi-infinite space. For a composite soil layer, the parameters of the different soil layers can be equivalent in the analysis. The calculation model is depicted in Fig. 2.

The horizontal displacement $U_{x,A}$ of point A caused by horizontal concentrated force $P_{x,B}$ at point B in semi-infinite space is expressed as Eq. (3)

$$U_{x,A}=K_x\cdot P_{x,B} \tag{3}$$

$$K_x=\frac{1}{16\pi G\left(1-v_d\right)}\left[\begin{array}{l}\frac{3-4v_d}{R_1}+\frac{1}{R_2}+\frac{X^2}{R_1^3}+\\ \frac{\left(3-4v_d\right)X^2}{R_2^3}+\frac{2wz}{R_2^3}\left(1-\frac{3X^2}{R_2^3}\right)+\\ \frac{4\left(1-v_d\right)\left(1-2v_d\right)}{R_2+Z_2}\left(1-\frac{X^2}{R_2\left(R_2+Z_2\right)}\right)\end{array}\right] \tag{4}$$

where v_d is the soil layer equivalent Poisson's ratio, G is the equivalent shear modulus of the soil layer, x, y, and z denote the coordinates of the displacement calculation point A, respectively, and u, v, and w denote the coordinates of the loading point B, respectively; $X=x-u$, $Y=y-v$, $Z_1=z-w$, $Z_2=z+w$, $R_1=\sqrt{X^2+Y^2+Z_1^2}$, $R_2=\sqrt{X^2+Y^2+Z_2^2}$

Supposing that a virtual force is applied on the boundary of the retaining structure of the foundation pit, as shown in Fig. 3, the integral Eq. (3) is integrated along the boundary, and the following boundary integral Eq. (5) can be constructed.

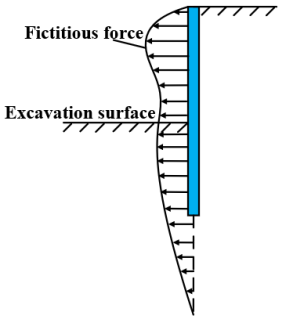

Fig. 3 Virtual forces on the pit boundary

$$U_{x,A} = \int_L K_x \cdot P_{x,B} dL \tag{5}$$

where L is the boundary of the foundation pit, and $P_{x,B}$ is the virtual force acting on point B on L.

If L is sufficiently subdivided, it can be considered that the virtual force on each segment is uniformly distributed, and Eq. (6) can be rewritten as follows

$$U_{x,A} = \sum_{i=1}^{m} P_{x,B,i} \cdot \int_{L_i} K_{x,i} dL_i \tag{6}$$

In the formula, L_i is the i-th segment of L; $P_{x,B,i}$ is the horizontal uniform concentrated force acting on the i-section, i = 1~m, where m is the total number of segments of the foundation pit boundary.

By considering the calculated horizontal displacement of the diaphragm wall as the actual displacement boundary condition and assuming point A is located on the boundary, we can derive the following matrix expression from Eq. (6).

$$\begin{bmatrix} U_{x,A,1} \\ \vdots \\ U_{x,A,j} \\ \vdots \\ U_{x,A,m} \end{bmatrix} = \begin{bmatrix} G_{11} & \cdots & G_{1j} & \cdots & G_{1m} \\ \vdots & \ddots & \vdots & \iddots & \vdots \\ G_{j1} & \cdots & G_{jj} & \cdots & G_{jm} \\ \vdots & \iddots & \vdots & \ddots & \vdots \\ G_{m1} & \cdots & G_{mj} & \cdots & G_{mm} \end{bmatrix} \cdot \begin{bmatrix} P_{x,B,1} \\ \vdots \\ P_{x,B,j} \\ \vdots \\ P_{x,B,m} \end{bmatrix} \tag{7}$$

where $G_{ji} = \int_{L_i} K_{x,i} dL_i$.

Eq. (7) can be abbreviated as follows

$$P_{x,B} = G^{-1} \cdot U_{x,A} \tag{8}$$

In this formula, the matrix G and the actual boundary conditions $U_{x,A}$ are known. we can calculate the virtual horizontal additional stress $P_{x,B}$ on the boundary of the foundation pit.

2.3 Calculation of the horizontal displacement and additional soil stress near the isolation pile

By utilizing the calculated additional horizontal stress on the boundary of the foundation pit, we can calculate the horizontal displacement of the free soil near the isolation pile. This can be achieved by integrating Eq. (9) along the depth of the load, as illustrated in Fig. 4.

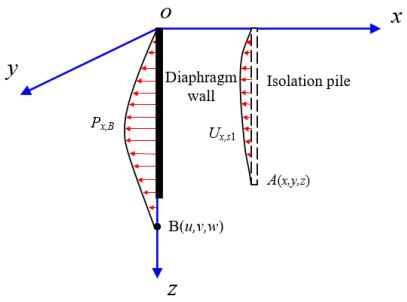

Fig. 4 Calculation model

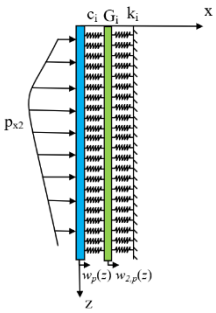

Fig. 5 Pile–soil interaction model under a Kerr foundation

$$U_{x,s1} = \int K_x \cdot P_{x,B} dw \tag{9}$$

In the formula, $P_{x,B}$ is the additional stress at the position of the diaphragm wall caused by the horizontal displacement of the diaphragm wall, and $U_{x,s1}$ is the horizontal displacement of the free soil at the position of the isolation pile caused by the excavation of the foundation pit when there is no isolation pile.

$$P_{x,s1} = kU_{x,s1} - GU''_{x,s1} \tag{10}$$

3. Horizontal displacement calculation of the isolated pile group

3.1 Horizontal displacement of a single pile

As shown in Fig. 5, the pile–soil interaction model under the Kerr foundation is established. The pile foundation is assumed to be a longitudinal circular cross-section Euler–Bernoulli beam with a diameter of d_p and a stiffness of E_pI_p, and the deflection differential equation for solving the horizontal displacement $w_{2,p}$ of the isolation pile is established.

$$\begin{aligned} &-\frac{E_p I_p G_i}{d_p c_i} \frac{d^6 w_{2,p}}{dz^6} + \frac{E_p I_p \left(c_i + k_i\right)}{dc_i} \frac{d^4 w_{2,p}}{dz^4} \\ &-G_i \frac{d^2 w_{2,p}}{dz^2} - k w_{2,p} = -P_{x,s1} \end{aligned} \tag{11}$$

In Eq. (11), $w_{2,p}$ represents the horizontal displacement of the shear layer spring, $P_{x,s1}$ represents the additional stress acting on the pile foundation. Using the finite

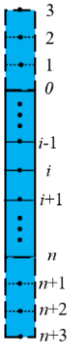

Fig. 6 Discretization of an isolated pile element

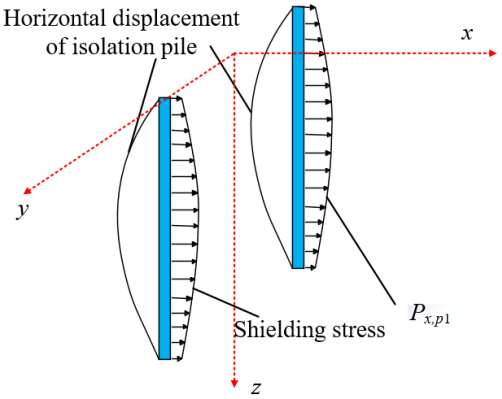

Fig. 7 Deformation force diagram of the pile group

difference method, Eq. (11) can be transformed into the following

$$\begin{aligned} &A(w_{2,p})_{i-3}+B(w_{2,p})_{i-2}+C(w_{2,p})_{i-1}\\ &+D(w_{2,p})_i+C(w_{2,p})_{i+1}+B(w_{2,p})_{i+2}\\ &+A(w_{2,p})_{i+3}=-p_{x,s1,i} \end{aligned} \tag{12}$$

where i = 0,1, ... , n; A, B, C, and D are all simplified coefficients of Eq. (11), $(w_{2,p})_i$ is the displacement of the shear layer of the foundation at the i-th node of the isolation pile, and $P_{x,s1}$, i is the additional stress at the i-th node of the isolation pile caused by the horizontal displacement of the diaphragm wall. By utilizing the principles of differential analysis, we observe the following characteristics

$$\begin{bmatrix} A\\ B\\ C\\ D \end{bmatrix}=\begin{bmatrix} 1 & 0 & 0 & 0\\ -6 & -1 & 0 & 0\\ 15 & 4 & 1 & 0\\ -20 & -6 & -2 & 1 \end{bmatrix}\times\begin{bmatrix} E_pI_pG_i/d_pc_il^6\\ E_pI_p(c_i+k_i)/d_pc_il^4\\ G_i/l^2\\ k_i \end{bmatrix} \tag{13}$$

In Eq. (13), l is the length of the differential node element, and L is the length of the isolation pile: l=L/n. The isolation pile is discretized with n + 7 node elements (there are six virtual elements at the beginning and end), and the discretization of the isolation pile is shown in Fig. 6.

For a case in which the bottom of the isolation pile is situated in the granite stratum and considered as the fixed end, while the pile top is free and the pile end is fixed, the following boundary conditions apply (Zhang *et al.* 2016).

When z = H (at the top of the pile), the displacement is 0, the rotation angle is 0. When z = 0 (at the bottom of the pile), the bending moment is 0, and the shear force is 0. In addition to these boundary conditions, the boundary conditions of the two shear layers need to be considered.

$$[K]=\begin{bmatrix} D+2C+4B-8A & -4B-10A & 2B+2A & 2A & & & & & \\ C+2B+6A & D-B-2A & C-A & B & A & & & & \\ B-2A & C-A & D & C & B & A & & & \\ A & B & C & D & C & B & A & & \\ & & \ddots & \ddots & \ddots & \ddots & \ddots & \ddots & \ddots \\ & & & A & B & C & D & C & B & A\\ & & & & A & B & C & D & C & B\\ & & & & & A & B & C & D & C-A\\ & & & & & & A & B & C+A & D+B+8A \end{bmatrix}$$

For the shear layer, when z = 0, the internal force of the shear layer is 0. When z = H, the shear deformation of the shear layer is 0, and the rotation angle is 0.

According to the boundary conditions, the virtual nodes are eliminated, and the displacement equation of the shear layer is obtained

$$\{w_{2,p}\}=[K]^{-1}\cdot\{P_{x,s1}\} \tag{14}$$

Where, $\{w_{2,p}\}=\left[(w_{2,p})_0,(w_{2,p})_1,\cdots,(w_{2,p})_n\right]^T$,

$\{p_{x1}\}=\left[(p_{x,s1})_0,(p_{x,s1})_1,\cdots,(p_{x,s1})_n\right]^T$

The horizontal displacement of the shear layer of the isolation pile is calculated using Eq. (14), and the horizontal displacement of the isolation pile is calculated using Eq. (15)

$$\{w_p\}=\left(1+\frac{k_i}{c_i}\right)w_{2,p}-\frac{G_i}{c_i}\frac{d^2w_{2,p}}{dx^2} \tag{15}$$

3.2 Horizontal displacement calculation of an isolated pile group considering the sheltering effect

In the analysis of a horizontal active pile group, the stiffness of the individual pile is significantly greater than the stiffness of the surrounding soil. As a result, the displacement of the soil is constrained by the presence of the pile, leading to the shielding effect of the passive piles in the pile group on the soil displacement. Consequently, the deformation and stress of a single pile are reduced due to the mutual shielding among the piles. In a pile group foundation, the actual displacement of an individual pile foundation is equal to the sum of the displacement of a single pile and the shelter displacement of the pile group.

The shelter displacement acts in the opposite direction to the free displacement of the single pile, thereby compensating for its effects.

First, the pile–pile interaction of the two pile models is analyzed, and then it is extended to the whole pile group. The simplified model of the adjacent pile group is shown in Fig. 9. The horizontal displacement w_p of the isolated pile 1 is calculated using Eq. (15), and the horizontal displacement $U_{x,s1}$ of the free soil near the isolated pile 1 is calculated with Eq. (9). Then, the shelter displacement generated at pile 1 is calculated with Eq. (16).

$$\Delta U_{x,p1} = U_{x,s1} - w_p \tag{16}$$

As shown in Fig. 7, due to the interaction of pile–soil–pile, the sheltering displacement of isolation pile 1 produces sheltering stress at isolation pile 2, which limits the displacement of isolation pile 2. First, the sheltering stress $P_{x,p1}$ of isolation pile 1 is calculated. Subsequently, the displacement $U_{x,\,s2}$ of the free soil at two locations of the isolation pile under the action of the shielding stress of isolation pile 1 is calculated.

$$P_{x,p1} = k\Delta U_{x,p1} - G\Delta U_{x,p1}'' \tag{17}$$

$$\Delta U_{x,s2} = K_x \cdot P_{x,p1} \tag{18}$$

The free soil displacement $U_{x,s2}$ at isolation pile 2 is transformed into the shielding stress $P_{x,s2}$ and applied to isolation pile 2. The horizontal displacement w_{p2} of isolation pile 2 under the shielding stress condition generated by isolation pile 1 is calculated.

$$K_x = \frac{1}{16\pi G(1-v_d)}\left[\begin{array}{l}\dfrac{3-4v_d}{R_1}+\dfrac{1}{R_2}+\dfrac{X^2}{R_1^3}+\\ \dfrac{(3-4v_d)X^2}{R_2^3}+\dfrac{2wz}{R_2^3}\left(1-\dfrac{3X^2}{R_2^3}\right)\\ +\dfrac{4(1-v_d)(1-2v_d)}{R_2+Z_2}\\ \left(1-\dfrac{X^2}{R_2(R_2+Z_2)}\right)\end{array}\right]$$

$$\begin{aligned}&-\frac{E_pI_pG_i}{d_pc_i}\frac{d^6w_{2,p2}}{dz^6}+\frac{E_pI_p(c_i+k_i)}{dc_i}\frac{d^4w_{2,p2}}{dz^4}\\ &-G_i\frac{d^2w_{2,p2}}{dz^2}-kw_{2,p2}=-P_{x,s2}\end{aligned} \tag{19}$$

$$\{w_{p2}\} = \left(1+\frac{k_i}{c_i}\right)w_{2,p2} - \frac{G_i}{c_i}\frac{d^2w_{2,p2}}{dx^2} \tag{20}$$

Finally, through the superposition principle, the final horizontal displacement w_{pi} of the isolation pile i under the influence of the shielding effect of pile 1, pile 2,..., pile n is calculated.

$$w_{pi} = w_p - w_{p1} - \cdots - w_{p(i-1)} \tag{21}$$

4. Calculation of the post-pile settlement caused by foundation pit excavation

The boundary element method is used to invert the additional stress $P_{x,p}$ caused by the horizontal displacement of the isolation pile. The Mindlin vertical displacement solution of Eq. (22) is then used to calculate the surface settlement caused by the horizontal displacement of the pile group after application of the isolation pile. The calculation

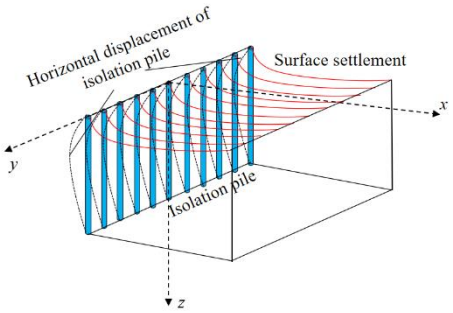

Fig. 8 Ground surface settlement behind the isolation pile

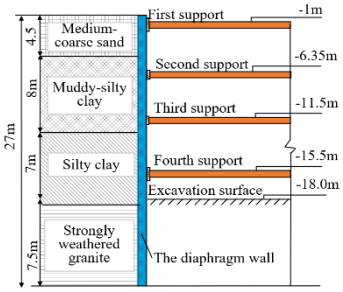

Fig. 9 Section of the foundation pit supporting structure

of the surface settlement after the isolation pile is installed is shown in Fig. 8.

$$w_z = \frac{P_{x,p}X}{16\pi G(1-v_d)}\left[\begin{array}{l}\dfrac{Z_1}{R_1^3}+\dfrac{(3-4v_d)Z_1}{R_2^3}\\ -\dfrac{6wzZ_2}{R_2^5}+\dfrac{4(1-v_d)(1-2v_d)}{R_2(R_2+Z_2)}\end{array}\right] \tag{22}$$

5. Introduction of finite element simulation

The South Gate subway station of Xiamen University serves as the study context. The retaining structure in this location consists of a diaphragm wall combined with an internal support system. The diaphragm wall was constructed using *C*30 concrete, with a depth of 27 m and a thickness of 1000 mm. The internal support system comprises four types of support. The first and second supports are concrete-based, spaced horizontally at 6 m, and possess an elastic modulus of 30 GPa. The third and fourth supports are steel supports with a diameter of 609 mm and a thickness of 16 mm, spaced horizontally at 3 m, and have an elastic modulus of 210 GPa. Regarding the isolation pile configuration, each pile has a length of 27 m and a diameter of 40 cm. The piles are spaced 0.8 m apart and possess an elastic modulus of 30 GPa. There are a total of 15 isolation piles, with a distance of 2 m between each pile and the diaphragm wall. As are shown in Figs. 9 and 10.

5.2 Spatial finite element model

The size of the foundation pit on the site is 200 m × 20 m × 19 m. In the spatial finite element model, the influence areas of the foundation pit excavation extend to four times

Table 1 Physical and mechanical parameters of the soil layers

Soil layer	Thickness/m	Gravity γ/(kN·m^{-3})	Cohesion c/kPa	Internal friction angle φ/°	Plasticity index I_p
Medium-coarse sand	4.5	21.6	0	27.8	19.21
Muddy-silty clay	8	17.8	8	11	21.37
Residual sand clay	7	19.6	24	15	13.3
Strongly weathered granite	50.5	19.2	28	18	11.4

Table 2 Weighted average mechanical parameters of the soil layers

Soil layer	Thickness/m	Gravity γ /(kN·m^{-3})	Cohesion c/kPa	Internal friction angle φ/°	Elastic modulus E/MPa	Poisson's ratio v
Weighted average parameters of soil layers	27	19.28	16.3	19.82	16.78	0.28

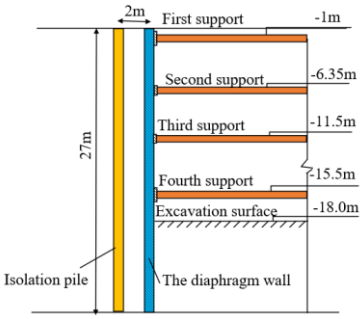

Fig. 10 Relative isolation pile position

the depth of excavation behind the diaphragm wall and two times the depth of excavation below the bottom of the pit. For computational efficiency, half the foundation pit's width is considered in the calculations. To create the final model, a 36 m segment of the foundation pit is selected lengthwise. As a result, the model size becomes 80 m × 36 m × 70 m, while the size of the actual foundation pit being modeled is 36 m × 10 m × 19 m.

The soil, diaphragm wall, isolation pile, and internal support are simulated by solid elements. A modified Cam-Clay constitutive is used for the soil, and a linear elastic constitutive is used for the diaphragm wall, isolation pile, and support. The interaction between soil and diaphragm wall, soil and isolation pile is realized by contact pairs, and the contact form is surface to surface contact (Avci *et al.* 2023, Ekmen *et al.* 2024). In this paper, the penalty function method is used to simulate the contact surface between the soil and diaphragm wall, soil and isolation pile (Algin *et al.* 2022). The master surface is the surface of diaphragm wall and isolation pile, the slave surface is the surface of soil.

These materials have the same geometric characteristics overlaying the contacting surfaces that can represent the deformable contact interface defined by the Coulomb friction model. The calculation and analysis types of the model are standard general static. The soil, diaphragm wall, isolation pile, and internal support all adopt a hex mesh, and the mesh is formed using a sweeping method. The algorithms are all medial axis algorithms, and the mesh type is C3D8. Before the soil mesh division, in order to ensure the mesh division near the isolation pile is regular, the soil near the isolation pile is partitioned. The mesh division near the isolation pile and the diaphragm wall is dense, and the farther away from the isolation pile and the diaphragm wall, the mesh is gradually sparse. At the same time, in order to ensure the calculation accuracy of the model, the mesh is gradually refined during the simulation process. When the calculation results of the two simulations are basically the same, the final mesh form is determined.

Because the bottom of diaphragm wall and isolation pile is in the rock layer, it is assumed that the diaphragm wall and the bottom of the isolation pile are fixed. The bottom of the model is the displacement/rotation boundary condition,which limits displacement in the three directions of x, y, z. The front and back of the model are displacement/rotation boundary conditions, which limit displacement in the y direction. The left and right sides of the model are displacement/rotation boundary conditions, which limit displacement in the x direction (Ekmen *et al.* 2023). The front and back of the diaphragm wall are displacement/rotation boundary conditions, which limit displacement in the y direction. The bottom of the diaphragm wall is the displacement/rotation boundary condition, which limits displacement in the x, y, and z directions. The bottom of the isolation pile is a displacement/rotation boundary condition, which limits displacement in the x, y, and z directions.

5.3 Engineering geology

The depth range of the diaphragm wall from top to bottom is medium-coarse sand, muddy-silty clay, residual sandy clay, and strongly weathered granite. The physical and mechanical parameters of each layer of soil are shown in Table 1. The weighted average physical and mechanical parameters for the soil layers are shown in Table 2.

The parameters of the modified Cam-Clay constitutive model can be converted using the existing parameters, and the conversion formula can be found in the literature (Ma and Ling *et al.* 2018), as shown in Table 3.

m buried depth of the isolation pile, and the maximum error

Table 3 Modified Cambridge intrinsic parameters for the soil layers

Soil layer	Logarithm of plastic bulk modulus λ	Stress ratio M	Logarithm of bulk modulus κ	Void ratio e	Poisson's ratio/v
Medium-coarse sand	0.186	1.10	0.0186	1.2	0.24
Muddy-silty clay	0.222	0.41	0.0222	0.68	0.3
Residual sand clay	0.089	0.57	0.0089	0.68	0.3
strongly weathered granite	0.0572	0.69	0.0057	0.62	0.25

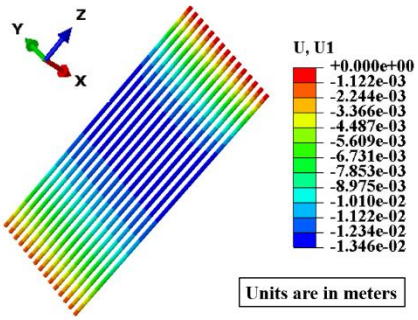

Fig. 11 Horizontal displacement of the isolation pile

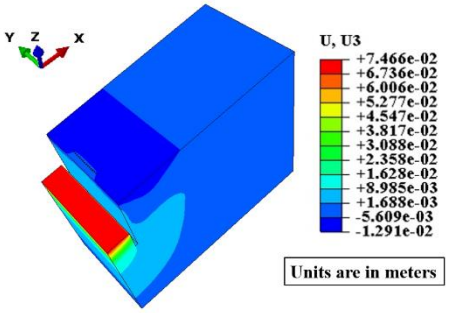

Fig. 12 Ground settlement nephogram

6. Theoretical prediction and numerical simulation

6.1 Theoretical verification

The numerical simulation results illustrate the horizontal displacement of the isolation pile and the surface settlement behind it, as depicted in Figs. 11 and 12, respectively. The horizontal displacement of the isolation pile exhibits a characteristic pattern of being comparatively larger in the middle and smaller at both ends. Concerning the surface settlement, there is an observed trend of initially increasing and subsequently decreasing settlement as the distance from the isolation pile becomes greater.

As shown in Fig. 13, in terms of the horizontal displacement of the isolation piles, the theoretical calculation results are compared with the numerical simulation results. The theoretical calculation results are similar to the numerical simulation results. The horizontal displacement of the isolation pile first increases and then decreases, showing a parabolic shape. The maximum horizontal displacements are 12.98 mm and 13.33 mm, respectively, and the error is only 2.6%. The depth of the maximum horizontal displacement is located at 13 m and 12 m, respectively. Although there is a certain error between the theoretical calculation result and the numerical simulation result when the buried depth is in the range of 0–12 m, the maximum error of the horizontal displacement at the same depth is 18.2%. However, since the research focus of this paper is on settlement control, the final calculated settlement result is very similar to the numerical simulation. Therefore, as an intermediate step, the calculation of the horizontal displacement of the isolation pile has a small error, which is acceptable. At the same time, the horizontal displacement of the numerical simulation and the theoretical calculation is very similar, in the range of 12–27

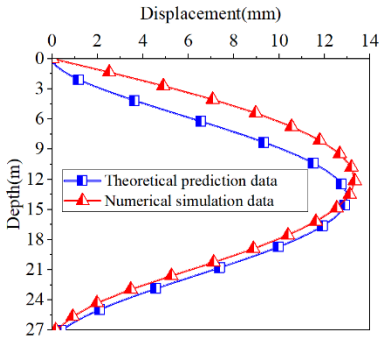

Fig. 13 Comparison of horizontal displacement

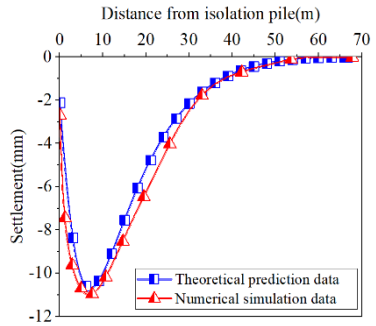

Fig. 14 Comparison of settlement after the isolation pile

is only 2.5%. Therefore, it is proven that the theoretical calculation method is reasonable.

As shown in Fig. 14, in terms of the surface settlement behind the pile, the theoretical calculation results are compared with the numerical simulation results. The theoretical calculation results are very close to the numerical simulation results. The maximum surface settlements are 10.8 mm and 11.3 mm, respectively, and the error is only 4.4%. The maximum surface settlements are

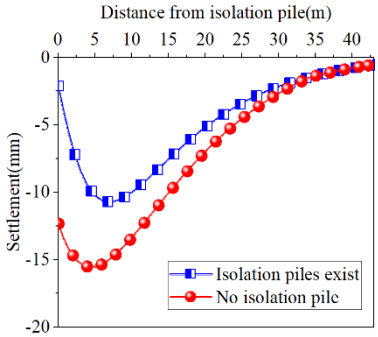

Fig. 15 Isolation effect of the isolation pile on settlement

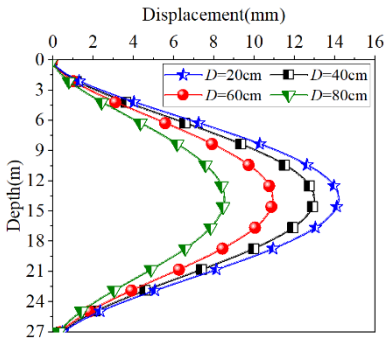

Fig. 16 Effect of pile diameter on horizontal displacement

located 6.5 m and 6.75 m from the isolation pile, respectively. The influence range of the surface settlement is about 55 m. At the same time, the change trend of the surface settlement curve shows a spoon shape, and the theoretical curve is in good agreement with the numerical simulation curve. It is proven that the theory in this paper has high accuracy in calculating the surface settlement behind the isolation pile.

6.2 Control effect of the isolation pile on the post-pile settlement

In Fig. 15, the theoretical analysis examines the effectiveness of employing an isolation pile in mitigating the surface settlement resulting from foundation pit excavation. Without the inclusion of an isolation pile, the maximum surface settlement is recorded as 15.5 mm, while the settlement at 2 m from the foundation pit (where the isolation pile is located) reaches 12.5 mm. However, when the isolation pile is implemented, the surface settlement is significantly reduced. The maximum surface settlement measures 10.7 mm, and the settlement at the exact position of the isolation pile is reduced to 2.4 mm. This represents a 31% reduction in the maximum settlement, indicating that the isolation pile effectively controls the surface settlement resulting from foundation pit excavation.

6.3 Influence of the isolation pile diameter

The standard construction parameters are isolation pile diameter D = 0.4 m, pile spacing S = 0.8 m, pile wall distance L =2 m, isolation pile elastic modulus E_P = 30 GPa, diaphragm wall thickness B =1 m, diaphragm wall diameter E_D =30 GPa. To analyze the influence of different parameters, the subsequent parameter analysis only changes a single variable, and the remaining values are standard parameters that will not be repeated in the future.

By keeping all other parameters unchanged, an analysis is conducted to assess the influence of the isolation pile diameter (D) on the horizontal displacement of the isolation pile and the resultant surface settlement. Fig. 16 illustrates the findings. Concerning the horizontal displacement of the isolation piles, as the pile diameter increases, the horizontal displacement gradually decreases, and the magnitude of the reduction becomes more pronounced. This indicates that increasing the pile diameter effectively controls the

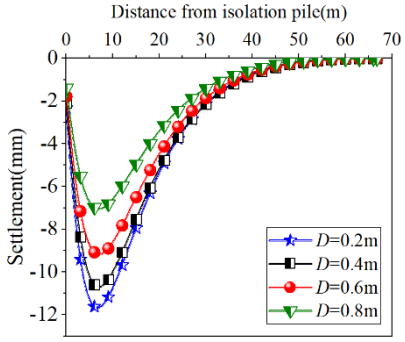

Fig. 17 Effect of pile diameter on settlement

horizontal displacement of the isolation piles. It should be noted that due to a pile spacing of 0.8 m, the maximum achievable pile diameter is 0.8 m where the isolation piles are in contact with each other. This configuration can achieve a minimum horizontal displacement of 8 mm, demonstrating the significance of the pile diameter in controlling horizontal displacement. Furthermore, the difference between the maximum and minimum horizontal displacements under different spacing conditions is 6 mm, accounting for 45.8% of the horizontal displacement observed under standard working conditions (D = 0.4 m).

This evidence underscores the substantial impact of the isolation pile diameter on controlling horizontal displacement.

As shown in Fig. 17, after application of the isolation piles with an increase in the pile diameter, the surface settlement decreases significantly, and the decrease increases. When the isolation piles are in contact with each other, that is, when the ultimate pile diameter is 0.8 m, the settlement after the pile is 7 mm, which is the settlement control limit of the isolation pile with a diameter of 0.8 m.

The difference between the maximum settlement and the minimum settlement under different isolation pile diameters is 4.9, which is 45.7% of the surface settlement under the standard working condition (D = 0.4 m), proving that the control effect of the isolation pile diameter on the settlement after the pile is very obvious.

6.4 Influence of isolation pile spacing

Keeping the other parameters unchanged, the spacing of the isolation piles is taken as S = 0.4 m, 0.8 m, 1.2 m, and 1.6 m, respectively, and the control effect of the spacing S

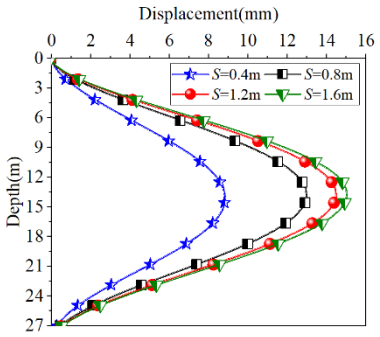

Fig. 18 Effect of pile spacing on horizontal displacement

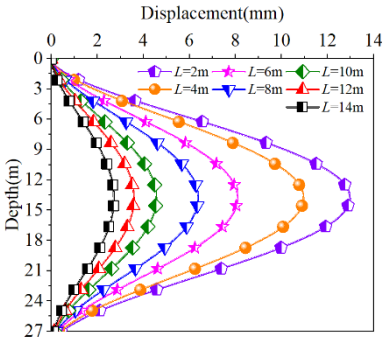

Fig. 20 Effect of pile wall distance

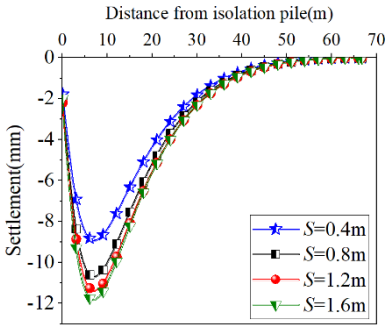

Fig. 19 Effect of pile spacing on settlement

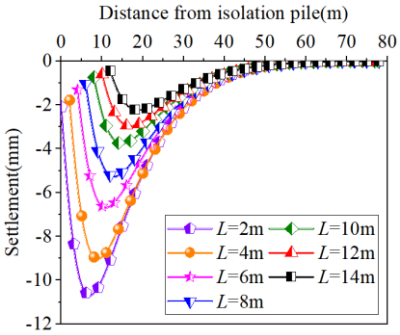

Fig. 21 Effect of pile wall distance on settlement

of the isolation piles on the horizontal displacement of isolation piles and the surface settlement behind the piles is analyzed. As shown in Fig. 18, in terms of the horizontal displacement of the isolation pile, the horizontal displacement of the isolation pile increases with the increase in the spacing of the isolation piles. When the spacing S of the isolation piles increases from 0.4 m to 0.8 m, that is, from 1 times the pile diameter to 2 times the pile diameter, the horizontal displacement of the isolation pile increases most significantly. When the spacing of the isolation piles increases from 0.8 m to 1.2 m, that is, from 2 times the pile diameter to 3 times the pile diameter, the horizontal displacement of the isolation piles increases, but the degree of increase is significantly lower than that from 1 times the pile diameter to 2 times the pile diameter. When the diameter of the isolation pile increases from 1.2 m to 1.6 m, the horizontal displacement of the isolation pile does not increase significantly, indicating that the control effect of the spacing corresponding to 3–4 times the diameter of the isolation pile on the horizontal displacement of the isolation pile gradually tends to be consistent. The spacing range with the most obvious control effect on the horizontal displacement of the isolation pile is 1 to 3 times the diameter of the isolation pile. The difference between the maximum horizontal displacement and the minimum horizontal displacement is 6.2 mm, which is 47.3% of the standard parameter (pile spacing S = 0.8 m). The spacing of the isolation piles is reduced, and the shielding effect between the piles increases. Therefore, reducing the spacing of the isolation piles can significantly reduce the horizontal displacement of the isolation piles themselves.

As shown in Fig. 19, in terms of surface settlement after installing the isolation piles, increasing the spacing of the isolation piles gradually increases the surface settlement.

When the pile spacing is 1–3 times the diameter of the isolation piles, the settlement control effect is better than that of more than 3 times the diameter of the isolation piles. The difference between the maximum settlement and the minimum settlement is 3.1 mm, which is 28.1% of the standard parameter (pile spacing S = 0.8 m). This shows that reducing the spacing of isolation piles can effectively reduce the surface settlement after installing isolation piles, and the settlement control effect is most obvious when the spacing of isolation piles is 1–3 times the diameter of the isolation piles.

6.5 Influence of the pile wall distance

In this study, the control effect of the pile wall distance (L) on both the horizontal displacement of the isolation pile and the surface settlement behind it is investigated while maintaining the other parameters constant. The pile wall distances tested are L = 2 m, L = 4 m, L = 6 m, L = 8 m, L = 10 m, L = 12 m, and L = 14 m. Fig. 20 shows that increasing the pile wall distance L results in a gradual reduction in the horizontal displacement of the isolation pile. For instance, when L is 2 m, the horizontal displacement measures 13.1 mm. However, when the pile wall distance reaches 10 m, the reduction in horizontal displacement is minimal, with only a 2 mm decrease from 10 m to 14 m. Notably, the difference in horizontal displacement between a pile wall distance of 2 m and 6 m is 5.1 mm. This suggests that the decrease in horizontal displacement is not linearly proportional to the pile wall distance but exhibits a nonlinear pattern. Initially, the reduction rate is rapid, followed by a slower decrease until stabilization occurs. The maximum difference in horizontal

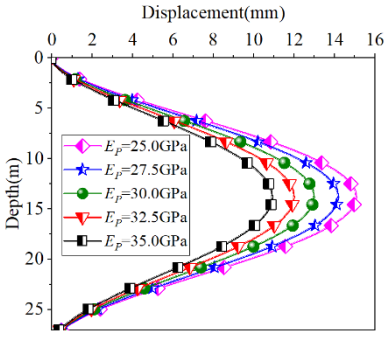

Fig. 22 Effect of elastic modulus of isolation pile

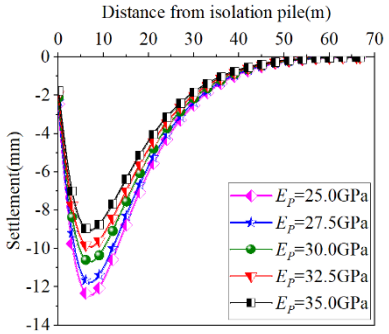

Fig. 23 Effect of elastic modulus of pile on settlement

displacement among different pile wall distances amounts to 10.7 mm.

Fig. 21 demonstrates the behavior of surface settlement after implementing the isolation piles. As the pile wall distance L increases, the overall surface settlement decreases. However, it is worth noting that the settlement at the isolation pile location increases. The control effect on surface settlement becomes more pronounced with larger pile wall distances. This can be attributed to the reduced horizontal displacement of the isolation pile resulting from increased pile wall distances, which enhances the isolating effect on surface settlement. The difference between the maximum and minimum settlements is 2.8 mm, accounting for 24.6% of the standard parameter (L = 2 m). This finding suggests that increasing the elastic modulus of the isolation pile effectively reduces the surface settlement behind the pile. Consequently, varying pile wall distances yield significant differences in the control effect on surface settlement after implementing isolation piles. Increasing the pile wall distance enhances the isolating effect of the piles, leading to better control of the surface settlement.

6.6 Influence of the elastic modulus of the pile

Keeping the other parameters unchanged, the elastic modulus of the isolation pile is E_P = 25 GPa, E_P = 27.5 GPa, E_P = 30 GPa, E_P = 32.5 GPa, and E_P = 35 GPa, respectively. The control effect of the elastic modulus E_P of the isolation pile on the horizontal displacement of the isolation pile itself and the surface settlement behind the pile is analyzed. As shown in Fig. 22, in terms of the horizontal displacement of the isolation pile increasing the elastic modulus of the isolation pile, the horizontal

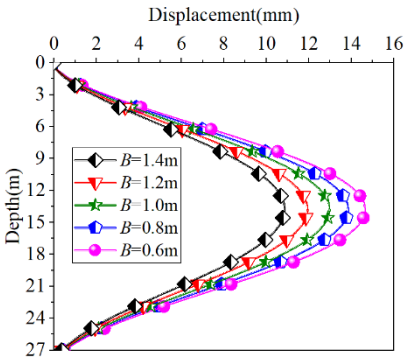

Fig. 24 Effect of diaphragm wall thickness

displacement of the isolation pile decreases, and the decreasing trend is uniform. The difference between the maximum horizontal displacement and the minimum horizontal displacement is 4.8 mm, which is 36.6% of the standard parameter (pile elastic modulus E_P = 30 GPa), indicating that increasing the elastic modulus of the isolation pile has a significant effect on the horizontal displacement of the isolation pile.

As shown in Fig. 23, with the increase of the elastic modulus of the isolation pile, settlement after the pile decreases significantly. The difference between the maximum settlement and the minimum settlement is 3.3 mm, which is 31.1% of the standard parameter (the elastic modulus of the pile E_P = 30 GPa), indicating that increasing the elastic modulus of the isolation pile can effectively reduce the surface settlement after the isolation pile.

6.7 Influence of the thickness of the diaphragm wall

Keeping the other parameters unchanged, the thickness of the diaphragm wall is B = 0.6 m, B = 0.8 m, B = 1.0 m, B = 1.2 m, and B = 1.4 m, respectively, and the control effect of the thickness of the diaphragm wall B on the horizontal displacement of the isolation pile itself and the surface settlement behind the pile is analyzed. As shown in Fig. 24, in terms of the horizontal displacement of the isolation pile, the thickness of the diaphragm wall is increased, and the horizontal displacement of the isolation pile under the same working condition is reduced, and the decreasing trend is uniform. This is because the increase in the thickness of the diaphragm wall reduces the horizontal displacement of the diaphragm wall, thereby reducing the additional stress acting on the isolation pile, resulting in a decrease in the horizontal displacement of the isolation pile. The difference between the maximum horizontal displacement and the minimum horizontal displacement is 4 mm, which is 30.5% of the standard parameter (B = 1 m), indicating that increasing the thickness of the diaphragm wall can reduce the horizontal displacement of the isolation pile. Comparing the control effect of increasing the thickness of the diaphragm wall and the diameter of the isolation pile on the horizontal displacement of the isolation pile, as shown in Figs. 24 and 16, increasing the same diameter of the isolation pile and the thickness of the diaphragm wall, the increase of the diameter of the isolation pile is more conducive to reducing the horizontal displacement of the isolation pile.

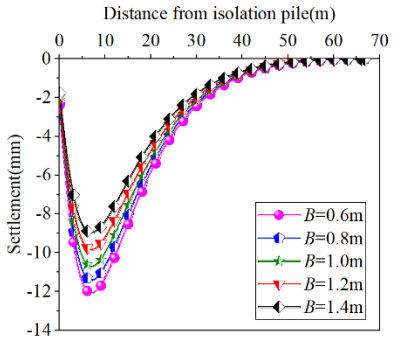

Fig. 25 Effect of diaphragm wall thickness on settlement

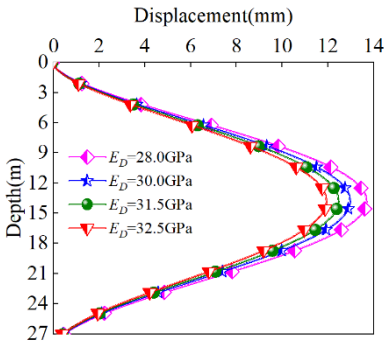

Fig. 26 Effect of the elastic modulus of the wall

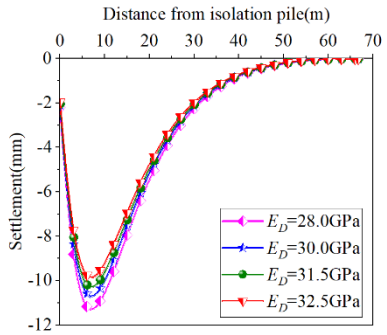

Fig. 27 Effect of the elastic modulus of the diaphragm

As shown in Fig. 25, in terms of surface settlement after installation of the isolation piles, increasing the thickness of the diaphragm wall can significantly reduce surface settlement after the isolation piles. This is because the increase in the thickness of the diaphragm wall reduces the horizontal displacement of the isolation piles, thereby reducing the additional stress generated by the horizontal displacement of the isolation piles and reducing the surface settlement after the isolation piles. The difference between the maximum settlement and the minimum settlement is 3 mm, which is 28% of the standard parameter (B = 1 m), indicating that increasing the thickness of the diaphragm wall can reduce surface settlement after the isolation pile. Comparing the control effect of increasing the thickness of the diaphragm wall and the diameter of the isolation pile on surface settlement after the isolation pile, as shown in Fig. 25 and Fig. 17, increasing the same diameter of the isolation pile and the thickness of the diaphragm wall, the increase of the diameter of the isolation pile is more conducive to reducing the surface settlement after the isolation pile.

6.8 Influence of the elastic modulus of the wall

As shown in Fig. 26, the elastic modulus of the diaphragm wall E_D is increased, the horizontal displacement of the isolation pile under the same working condition is reduced. This is because the elastic modulus of the diaphragm wall increases, and the horizontal displacement of the diaphragm wall decreases accordingly when the foundation pit of the same depth is excavated, thereby reducing the additional stress at the position of the isolation pile caused by the horizontal displacement of the diaphragm wall, resulting in a decrease in the horizontal displacement of the isolation pile. The difference between the maximum horizontal displacement and the minimum horizontal displacement is 1.9 mm, which is 14.5% of the standard parameter.

As shown in Fig. 27, in terms of surface settlement after installation of the isolation piles, increasing the elastic modulus of the diaphragm wall E_D can reduce the surface settlement. This is because the increase in the elastic modulus of the diaphragm wall reduces the horizontal displacement of the isolation piles, which in turn reduces the additional stress generated by the horizontal displacement of the isolation piles, thereby reducing the surface settlement after the isolation piles are installed. The difference between the maximum settlement and the minimum settlement is 1.7 mm, which is 15.9% of the standard parameter.

6.9 Comprehensive comparison of different construction parameters

The effects of different parameters are comprehensively compared, including the diameter, elastic modulus, and spacing of the isolation pile, the distance between the isolation pile and the wall, the diameter and elastic modulus of the diaphragm wall, the number of internal supports, and the diameter of the internal support. The standard construction parameters are used as the standard (D = 0.4 m, S = 0.8 m, L = 2 m, E_P = 30GPa, B = 1 m, E_D = 30 GPa).

Control a single variable, the variables are commonly used in on-site construction parameters. In the case of the parameters selected in this paper, the control effects of the diameter, spacing, elastic modulus of the isolation pile, the thickness and elastic modulus of the diaphragm wall on the horizontal displacement of the isolation pile are 6 mm, 6.2 mm, 4.8 mm, 4 mm, 1.9 mm, 3.8 mm, 1.1 mm, respectively. These values are 46.2%, 47.7%, 36.6%, 30.5%, 14.5%, 29%, 8.4% of the standard conditions, respectively. The control values of surface settlement are 4.9 mm, 3.1 mm, 3.3 mm, 3 mm, 1.7 mm, which are 45.4%, 28.7%, 30.6%, 27.8%, 15.7% of the standard conditions, respectively. In summary, compared with controlling the construction parameters of the foundation pit retaining structure, controlling the construction parameters of the isolation piles has a better control effect on the horizontal displacement of the isolation piles and surface settlement. Under common on-site construction parameters, increasing the diameter and

elastic modulus and reducing the spacing of the isolation piles are the most effective means to control the horizontal displacement of the isolation piles and surface settlement. Changing the diameter and elastic modulus of the diaphragm wall can reduce the horizontal displacement of the isolation pile and surface settlement, but the effect is poor compared to directly changing the parameters of the isolation piles.

7. Conclusions

This paper utilizes a combination of theoretical calculations and numerical simulations to analyze the effect of isolation piles on surface settlement resulting from foundation pit excavation. The specific conclusions obtained from this study are as follows:

• The prediction theory of horizontal displacement of isolation pile caused by foundation pit excavation is established, based on the calculated horizontal displacement of diaphragm wall, and the additional stress near the isolation pile is obtained by combining boundary element method and Mindlin solution. Compared with the numerical simulation results, the horizontal displacement law is similar. The maximum horizontal displacement is only 0.35 mm, the error is only 2.6%. The depth of the maximum horizontal displacement is basically the same, at 12 m and 13 m respectively, which proves that the calculation theory in this paper is reasonable.

• The calculation theory of soil surface settlement after isolation pile is established, and the additional stress field near the isolation pile is inverted by using the horizontal displacement of the isolation pile combined with the boundary element method, and the surface settlement after the isolation pile is calculated by using the Mindlin solution. Compared with the numerical simulation results, the variation trend of surface settlement is basically the same. The maximum surface settlement is 10.8 mm and 11.3 mm respectively, and the error is only 4.4%. The maximum surface settlement is located at 6.5 m and 6.75 m away from the isolation pile respectively, and the error is only 0.4%, which proves that the theory of this paper is reasonable.

• In the case of selecting the parameters in this paper, the control of the horizontal displacement of the isolation pile by the diameter, spacing, elastic modulus of the isolation pile, the thickness and elastic modulus of the diaphragm wall are 6 mm, 6.2 mm, 4.8 mm, 4 mm, 1.9 mm, respectively, which are 46.2%, 47.7%, 36.6%, 30.5%, 14.5% of the standard conditions. The control amounts of surface settlement are 4.9 mm, 3.1 mm, 3.3 mm, 3 mm, 1.7 mm, respectively, which are 45.4%, 28.7%, 30.6%, 27.8%, 15.7 of the standard conditions, respectively. This shows that optimizing the parameters of the isolation pile has the best control effect on the horizontal displacement of the isolation pile and surface settlement. Changing the diameter and elastic modulus of the diaphragm wall can reduce the horizontal displacement of the isolation pile and surface settlement, but the effect is poor compared to directly changing the parameters of the isolation piles.

Acknowledgments

The research described in this paper was financially supported by Science and Technology Plan of Fujian Provincial Department of Housing and Urban-Rural Development (Grant No. 2022K292). We are very grateful for the data and technical support of Xiamen Construction Engineering Co., Ltd. Of China Railway First Group, and the authors would like to thank reviewers for useful comments and editors for improving the manuscript.

References

Algin, H.M., Ekmen, A.B. and Kaya, E. (2022), "3D seismic response assessment of barrette piled high-rise building with comprehensive subsurface modelling", *Soil. Dyn. Earthq. Eng*., **163**(2022). https://doi.org/ 10.1016/j.soildyn.2022.107488.

Avci, Y. and Ekmen, A.B. (2023), "Artificial intelligence assisted optimization of rammed aggregate pier supported raft foundation systems based on parametric three-dimensional finite element analysis", *Structures*., **56**(2023). https://doi.org/10.1016/j.istruc.2023.105031.

Bilotta, E. and Taylor, R.N. (2005), "Centrifuge modelling of tunnelling close to a diaphragm wall", *Int. J. Phys. Model. Geo.*, **5**(1), 27-41. https://doi.org/10.1680/ijpmg.2005.050103.

Bilotta, E. (2008), "Use of diaphragm walls to mitigate ground movements induced by tunnelling", *Géotechnique.*, **58**(2), 143-155. https://doi.org/10.1680/geot.2008.58.2.143.

Bilotta, E. and Russo, G. (2011), "Use of a line of piles to prevent damages induced by tunnel excavation", *J. Geotech. Geoenviron.*, **137**(3), 254-262. https://doi.org/10.1061/(ASCE)GT.1943-5606.0000426.

Cao, L.Q., Chen, X.S., Shen, X., Zhang, D.L., Su, D. and Fang, H.C. (2022), "Theoretical analysis of the barrier effect of embedded isolation piles on tunneling-induced vertical ground displacements", *Comput. Geotech*., **144**(2022). https://doi.org/10.1016/J.COMPGEO.2021.104609.

Cao, L.Q., Chen, X.S., Lin, X.T., Su, D., Fang, H.C. and Lu, D.C.(2023), "Analytical solutions for the restraint effect of isolation piles against tunneling-induced vertical ground displacements", *J. Rock. Mech. Geotech.*, **15**(10), 2582-2596. https://doi.org/10.1016/J.JRMGE.2023.03.002.

Chen, R.P., Meng, F.Y., Li, Z.C., Ye, Y.H. and Hu, Q. (2016), "Considerable displacement and protective measures for metro tunnels adjacent deep excavation", *J. Zhejiang. Univ. (Eng. Sci)*., **50**(5), 856-863. https://doi.org/10.3785/j.issn.1008-973X.2016.05.007.

Chen, R.P., Ashraf, A.M. and Meng, F.Y. (2018), "Three-dimensional centrifuge modeling of influence of nearby excavations on existing tunnels and effects of cut-off walls", *Chin. J. Geotech. Eng.*, **40**(2), 6-11. https://doi.org/10.11779/CJGE2018S2002.

Cheng, Y.C., Gong, D.K., Ye, J.N. and Zheng, X. (2019), "Effect analysis of isolation piles outside foundation pit on controlling lateral soil displacement", *J. Disaster. Prevent. Mitigat. Eng.*, **39**(3), 478-486.

Ekmen, A.B., and Avci, Y. (2023), "Artificial Intelligence-Assisted Optimization of Tunnel Support Systems Based on the Multiple Three-Dimensional Finite Element Analyses Considering the Excavation Stages", *Ijst-t. Civ. Eng*., **47**(3), 1725-1747. https://doi.org/ 10.1007/s40996-023-01109-7.

Ekmen, A.B. and Avci, Y. (2024), "Development of novel artificial intelligence functions based on 3D finite element method using February 6 Kahramanmaraş Seismic Records for earthquake effects prediction in various soils", *Eng. Geol.*, **336**(2024),

107570. https://doi.org/ 10.1016/j.enggeo.2024.107570.
Farhangi, V. and Karakouzian, M. (2020), "Effect of fiber reinforced polymer tubes filled with recycled materials and concrete on structural capacity of pile foundations", *Appl. Sci. Basel.*, **10**(5). https://doi.org/10.3390/app10051554.
Huang, K., Sun, Y.W., Kuang, X.L., Huang, X.Q., Liu, R.N. and Wu, Q.J. (2022), "Study on the restraint effect of isolation pile on surface settlement trough induced by shield tunnelling", *Appl. Sci.*, **12**(10), 4845-4845. https://doi.org/10.3390/APP12104845.
Kerr, A.D. (1985), "On the Determination of Foundation Model Parameters", *J. Geotech. Eng.*, **111**(11), 1334-1340. https://doi.org/10.1061/(asce)0733-9410(1985)111:11(1334).
Ledesma, A. and Alonso, E.E. (2017), "Protecting sensitive constructions from tunnelling: the case of world heritage buildings in Barcelona", *Géotechnique*, **67**(10), 914-925. https://doi.org/10.1680/jgeot.SiP17.P.155.
Li, T., Yang, M. and Chen, X. (2023a), "A Simplified Analytical Method for the Deformation of Pile Foundations Induced by Adjacent Excavation in Soft Clay", *Buildings.*, **13**(8),1919-. https://doi.org/10.3390/BUILDINGS13081919.
Li, T., Yang, M. and Chen, X. (2023b), "Lateral deformation response of an adjacent passive pile under the combined action of surcharge loading and foundation excavation", *Sustainability*, **15**(18). https://doi.org/10.3390/SU151813619.
Ling, F.M., Chen, G.X. and Liu, X.Z. (2018), "Deformation characteristics of suspended curtain deep foundation pit of metro lines", *Chin. J. Geotech. Eng.*, **40**(12), 2182-2190. https://doi.org/10.11779/CJGE201812004.
Luca, M. and Sebastiano, R. (2021), "Predicted and observed behaviour of pre-installed barriers for the mitigation of tunnelling effects", *Tunn. Undergr. Sp. Tech.*, **118**. https://doi.org/10.1016/J.TUST.2021.104200.
Ma, H.L. and Liang, F.Y. (2018), *Foundation Pit Engineering*, Tsinghua University Press, Beijing, China.
Mindlin, R.D. (1936), "Force at point in the interior of a semi-infinite solid", *Physics*, **7**(1936), 195-202. https://doi.org/10.1063/1.1745385.
Pasternak, P.L. (1954), *Fundamentals of a New Method of Analyzing Structures on an Elastic Foundation By Means of Two Foundation Constants*, Gosudarstvennoe Izdatelstro Liberaturi po Stroitelstvui Arkhitekture, Moscow, Russia.
Rampello, S., Fantera, L. and Masini, L. (2019), "Efficiency of embedded barriers to mitigate tunnelling effects", *Tunn. Undergr. Sp. Tech.*, **89**(2019), 109-124. https://doi.org/10.1016/j.tust.2019.03.027.
Stone, R.C., Farhangi, V. and Karakouzian, M.A. (2023), "A novel short pile foundation system bonded to highly cemented layers for settlement control", *Can. Geotech. J.*, **60**(9), 1332-1351. https://doi.org/10.1139/cgj-2020-0710.
Tanahashi, H. (2004), "Formulas for an Infinitely Long Bernoulli-Euler Beam on the Pasternak Model", *Soils. Found.*, **44**(5), 109-118. https://doi.org/10.3208/sandf.44.5_109.
Vesic, A.S. (1961), "Bending of beams resting on isotropic elastic solids", *J. Soil. Mech. Found. Eng.*, **87**(2), 35-53. https://doi.org/10.1061/JMCEA3.0000212.
Xu, C.J. and Luo, Z.Y. (2011), "Internal force and deformation analysis of pile-brace support structure of foundation pit considering deformation compatibility", *Appl. Mech. Mater.*, **1446**(90-93), 446-452. https://doi.org/10.4028/www.scientific.net/AMM.90-93.446.
Yao, W.J. and Yin, W.X. (2010), "Numerical simulation of a super-Long pile group under both vertical and lateral loads", *Adv. Struct. Eng.*, **13**(6), 1139-1151. https://doi.org/10.1260/1369-4332.13.6.1139
Zhang, Z.G., Huang, M.S., Zhang, C.P. and Lu, M.H. (2019), "Time-domain analyses for pile deformation induced by adjacent excavation considering influences of viscoelastic mechanism", *Tunn. Undergr. Sp. Tech.*, **85**(2019), 392-405. https://doi.org/10.1016/j.tust.2018.12.020.
Zhang, Z.G., Lu, M.H., Xu, C., Gong, J.F. and Zhao, Q.H. (2016), "Simplified Solution for Tunnelling-Induced Pile Foundation Deformation Based on the Kerr Foundation Model", *Mod. Tunn. Technol.*, **53**(6), , 55-66. https://doi.org/10.13807/j.cnki.mtt.2016.06.009.
Zhao, C., Feng, Y., Wang W.J. and Niu, Z.J. (2023), "Mechanical properties and numerical analysis of underground continuous wall in underground grain silo foundation pit", *Buildings*, **13**(2), 293-293. https://doi.org/10.3390/BUILDINGS13020293.
Zheng, G., Du, Y. and Diao, Y. (2015), "Optimization analysis of efficiency of isolation piles in controlling the deformation of existing tunnels adjacent to deep excavation", *Chin. J. Rock. Mech. Eng.*, **34**(1), 3499-3509. https://doi.org/10.13722/j.cnki.jrme.2014.0235.
Zhu, Y.P., Wu, L.P., Shi, D.B., Zhao, Z.F., Lv, X.X. and Duan, X.G. (2022), "Application of nonlinear soil resistance-pile lateral displacement curve based on Pasternak foundation model in foundation pit retaining piles", *Rock. Soil. Mech.*, **43**(9), 2581-2591. https://doi.org/10.16285/j.rsm.2021.193.

CC